CHEMISTRY OF MATERIALS

Article

pubs.acs.org/cm

Graphene Amplification by Continued Growth on Seed Edges

Lin Gan, Xuewu Ou, Qicheng Zhang, Ruizhe Wu, and Zhengtang Luo*

Department of Chemical and Biomolecular Engineering, The Hong Kong University of Science and Technology, Clear Water Bay, Kowloon, Hong Kong

Supporting Information

ABSTRACT: Large-area single-layer graphenes with high crystallinity are desired for electronic applications. Here we demonstrate a continued growth method to amplify an existing graphene seed, originally grown by chemical vapor deposition, by preferentially inducing nucleation at seed edges. More specifically, this approach involves a surface oxidation step after the first growth, which leads to the observed formation of oxides at the vicinity of graphene edges, along with the inevitable formation of cracks due to oxidation, and thus limit growth predominantly at those edges, as a consequence of the reduced energy barrier of methane decomposition by oxygen moieties. Consequently, we successfully grow millimeter-size secondary single-crystal graphene structures with the same lattice structure and orientation as the original seeds. Selected area electron diffraction (SAED), Raman spectroscopy characterization, along with electronic transport measurement confirmed the structure coherence after the regrowth, even in the seed/regrown grains boundary region. This clone-like method provides a venue for production of graphene electronics with reproducible properties.

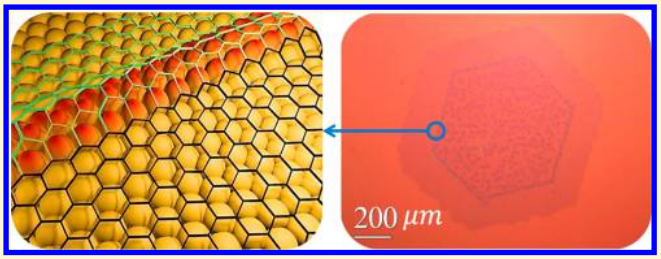

INTRODUCTION

Graphene has spawned widespread interests from the whole world for its potential application in electronics. To fabricate graphene-based devices with quality that meets current silicon industrial standards, however, graphene sheets with high crystallinity, reproducible structures, and defined crystal orientations are required, which are still challenges for graphene synthesis. Among all graphene growth methods, chemical vapor deposition (CVD) on copper foil/film[1] can produce a significant fraction of monolayer graphene.[2] However, during the nucleation stage of this type of growth, due to the statistical nature of the nuclei formed by random-distributed irregularities, impurities, and copper grain boundaries,[3,4] such synthesized graphenes suffer from limited grain size and lacking of orientation correlation in long ranges.[5] Our recent work, along with many other's work,[6−8] has shown that the size of single-crystal graphene can be significantly increased to subcentimeter, if the nucleation density could be controlled during the nucleation stage, thus allowing ample space for graphene growth.

On the other hand, regrowth from an existing graphene seed, or continued growth[9] would allow replication of the seed lattice and orientation, thus become an promising alternative to enlarge graphene sizes. For this purpose, a variety of techniques, such as heteroepitaxial growth[10] and extended growth,[11,12] have been developed, however, with only limited successes by producing regrown graphene flakes of several microns in size for inability to control nucleation sites. In alignment with continued-growth chemistry, the combined utilization of our aforementioned techniques to limit nucleation sites[8] provides an opportunity to amplify the graphene flake into even much larger size while maintaining their structure coherence. Unlike previously reported two-step CVD process,[11,12] here we demonstrate a novel continued growth technique, which involves introducing oxides along graphene seeds edges, together with our previously reported nucleation density control technique, which enables us to replicate the lattice structure and orientation of an existing graphene flake, meanwhile, to amplify the graphene seed to millimeter size. The key step in this work is the mild oxidation surface treatment used between the first and second CVD processes, which induces oxides around the edges of existing seed but inevitably also on interior cracks of those seeds. Those oxides reduce the energy barrier for nucleation during the second growth step and thus allow the continued growth to be confined in localized regions (i.e., mostly seed edges) as opposed to other two-step CVD processes, where new nucleation centers are randomly generated. Consequently, we were able to amplify the size of the existing seed from a few hundreds of microns to millimeter scale. The power of this experimental method is its ability to control the microenvironment of nucleation sites which lead to the continued growth occurring preferentially on the edges of graphene seeds. We believe that this general strategy can be extended to an enormous range of 2D materials preparation and has broad impact on 2D material-based nanoelectronics.

Received: April 3, 2014
Revised: July 4, 2014
Published: July 7, 2014

   dx.doi.org/10.1021/cm501184s | Chem. Mater. 2014, 26, 4137−4143

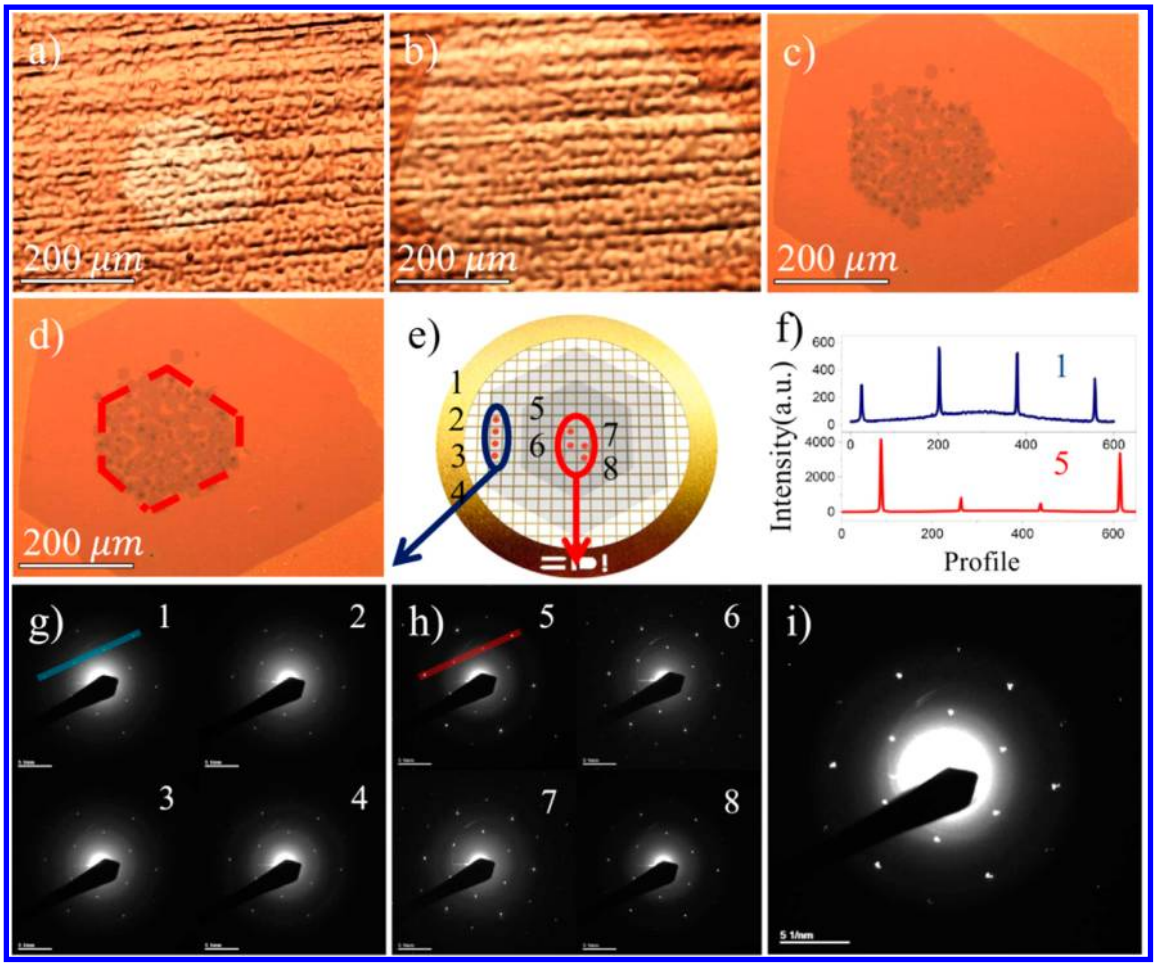

Figure 1. Continued growth of graphene. (a) Optical image of CVD-grown graphene seed and (b) the regrown grain. Both samples are visualized by oxidation method (see text). (c) Optical image of regrown grain transferred onto silicon wafer. (d) Image in (c) overlapped with outline of seed in (a). (e) A schematic view of the sampling location for SAED. Dots and arrows show the selected locations of SAED patterns. (f) SAED intensity profiles of (g) regrown and (h) seed grains, respectively. (i) Overlapped SAED patterns for eight locations in (g) and (h).

EXPERIMENTAL SECTION

Synthesis of Graphene Seeds by First Chemical Vapor Deposition (CVD). Graphene seeds were prepared by atmospheric pressure CVD (APCVD) on copper foil (Alfa Aesar, stock no.13382) with a reported method.[8]

Surface Treatment to Introduce Oxides. A fast heating process was used to introduce desired oxide morphology. Graphene/Cu sample prepared in the first CVD process was loaded into a CVD chamber, equipped with a quartz tube of approximate double length of the furnace, then purged with 320 sccm Argon (Hong Kong Specialty Gases Co., LTD, 99.999%, oxygen concentration <3 ppm) for 20 min. Next, temperature was ramped to 1050 °C while the furnace is seated away from the sample. After temperature stabilization, we quickly moved the furnace onto the graphene/Cu to oxidize the surface with the trace amount of oxygen in the system. After the desired oxidation were obtained by finely tuning the oxidation duration, we then charged the system with 21 sccm hydrogen (Hong Kong Specialty Gases Co., Ltd, 99.999%, oxygen concentration <5 ppm) and 15 sccm methane (500 ppm methane diluted in argon, Arkonic Gases and Chemicals, Inc., 99.99%) and started the second graphene growth. The extension of oxidation was not a key factor in regulating the regrowth as we did not observe significant variation of the regrown part, both for the coppers oxidized in the trace-oxygen-contained system and in air (i.e., at oxygen concentration of ∼209 460 ppm).

Graphene Transfer onto Silicon Wafer and TEM Copper Grid. The obtained graphene/Cu is spin coated with PMMA of ∼300 nm thickness (MicroChem Corp. 495 PMMA A6) and baked at 180 °C for 2 min. Samples are then cut into sizes of silicon substrate or TEM copper grid and etched in solution (10 g $FeCl_3$, 10 mL HCl, and 200 mL DI water) for ∼5 h. Residue on the sample is then immersed in DI water for removing of etching solvent (a few drops of HCl are added to control the pH). After that, silicon wafer or copper grid is used to scoop the PMMA membrane and dried on hot plate at 50 °C for 10 min. Finally, PMMA is removed by dipping into boiling acetone (for silicon wafer) for 1−2 min or in room temperature acetone for ∼10 min (for copper grid).

Electron Beam Lithography. FET devices were fabricated with E-beam lithography (Raith) with channel length of 20 μm and width of 50 μm.

Electron Transport Measurement. The electronic transport measurement was performed under vacuum (∼10^{-6} Torr) with 4155C semiconductor parameter analyzer (Agilent). The source-drain voltage is kept at 10 mV and the back gate is swept from −50 to 100 V.

Transmission Electron Microscopy and Selected Area Electron Diffraction (SAED). TEM images and SAED patterns were obtained using a JEOL 2010F operated at 200 keV.

Raman Spectroscopy and Optical Images. The Raman spectrum of single points and mapping were recorded with a Renishaw Raman RM3000 scope using a 514 nm excitation argon laser, the step interval for mapping is 1 μm. Optical images were taken by a LEICA DFC 290 optical microscope.

Atomic Force Microscopy. AFM was scanned under semicontact mode using a NTEGRA probe NanoLaboratory (NT-MDT, Inc.) with ACTA tips from AppNano at 1.5 Hz scan rate and 512 × 512 resolutions.

dx.doi.org/10.1021/cm501184s | *Chem. Mater.* 2014, 26, 4137−4143

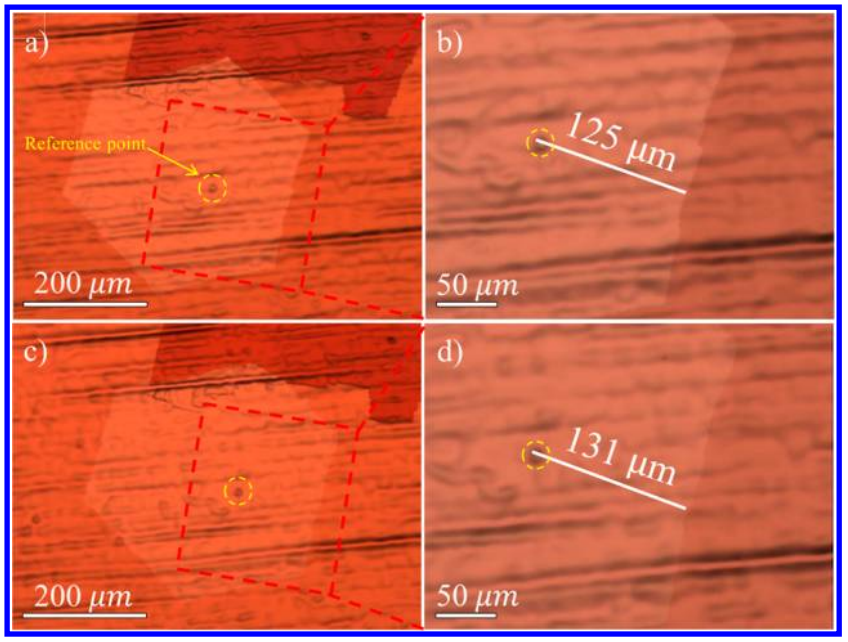

Figure 2. Optical images for seed and regrown grains. (a,c) Optical images of the seed and regrown grains on oxidized copper. (b,d) Magnified regions in (a) and (c). The regrowth time is ∼5 min. The straight edges before and after regrowth indicate that the edges grow uniformly outward during regrowth. The circled feature is used as a reference point.

■ RESULTS AND DISCUSSION

The continued growth process is schematically illustrated in Figure S1 of the Supporting Information. Basically, our process mainly consists of the following three processes: (1) a first CVD growth to produce ultralow density of single-crystalline graphene seeds; (2) a surface heating process to finely control oxidation on graphene/copper substrate for introducing morphologies that confine graphene growth occurring mainly on the edges of grains in the next step; and (3) a second CVD growth to enable the preferential regrowth at the graphene seeds edges, which enables the regrown flake to inherit the seed lattice structure and orientation, contrary to random formation of new nuclei on Cu surface in a two-step CVD process.[11,12] Unlike reported doping or isotope growth,[13−15] where only a single CVD growth process is used, however, this continued growth involves two independent and complete CVD processes(i.e., sample surface temperature was risen and cooled in two separated CVD growths) with a surface treatment step involved. As will be clearly seen from morphology investigation, this surface treatment step is critical in the amplification of graphene grains, which enables the second CVD graphene growth to confine mainly to the edge of graphene flakes and lead to size amplification.

Figure 1 illustrates the optical images of graphene at various stages in the preparation (see Figure S2 in Supporting Information). Figure 1a shows a large graphene seed that was prepared by the ultralow density-control method reported in our recent work, which enables us to lower the graphene flake density to 0.1 nuclei/mm^2, as opposed to 5000−10 000 nuclei/mm^2 in conventional CVD graphene grown on Cu.[8] More specifically, hydrogen supply is turned off (i.e., only argon is used as carrier gas) to form a trace-oxygen environment during the heating process, which leads to the formation of an ultralow density of copper nanoparticles with certain height on the surface. Those nanoparticles reduce the nucleation energy barrier and thus become the localized center during the subsequent growth, achieving ultralow graphene flake density. Other than switching off the hydrogen supply, the rest of the growth procedure is similar to conventional methods. With this method, ultralow nucleation density ensures each grain has enough space to grow and thus enables us to control the graphene grain size. Moreover, here we used the oxidation assisted visualization method, which enables us to see the graphene flake on the copper substrate.[16] Figure 1b depicts the graphene flake obtained with this continued growth method, the diameter of the flake appears to be amplified from ∼200 to ∼500 μm after the regrowth, while the same position, shape and orientation as the original seeds are still maintained, as shown in Figure 1a (for more examples, see Figure S3 in Supporting Information). The shape of the grain slightly deviated from strict hexagon, probably due to the hydrogen etching effect,[17] or resulted from various lattice orientation of the underneath copper substrate.[18] After transferring onto a 300 nm oxide silicon wafer, as shown in Figure 1c, however, the regrown graphene flake exhibits two distinctive contrast regions, that is, a hexagon at the center and a hexagon ring at the periphery (for more examples, see Figure S4 in Supporting Information). Closer inspection of the center hexagon region reveals that it mainly comprises small hexagon graphene structures underneath a large graphene membrane that is connected to the regrown film. Predominantly, as shown in Figure 1d, hexagon at the center exactly matches with the seed graphene in Figure 1a, providing strong evidence to support that the regrown graphene rooted in the original seed graphene.

To accurately determine and validate the structures of the seed and regrown regions, we investigated the lattice structure at many random selected positions by selected area electron diffraction (SAED). We analyzed samples at four locations (∼40 μm apart) in the seed and regrown regions, respectively, schematically depicted in Figure 1e (see Figure S5 for more examples). SAED patterns at all four locations in the regrown region (Figure 1g) show sharp diffraction patterns with identical hexagonal symmetry, typical for single-crystal

dx.doi.org/10.1021/cm501184s | Chem. Mater. 2014, 26, 4137−4143

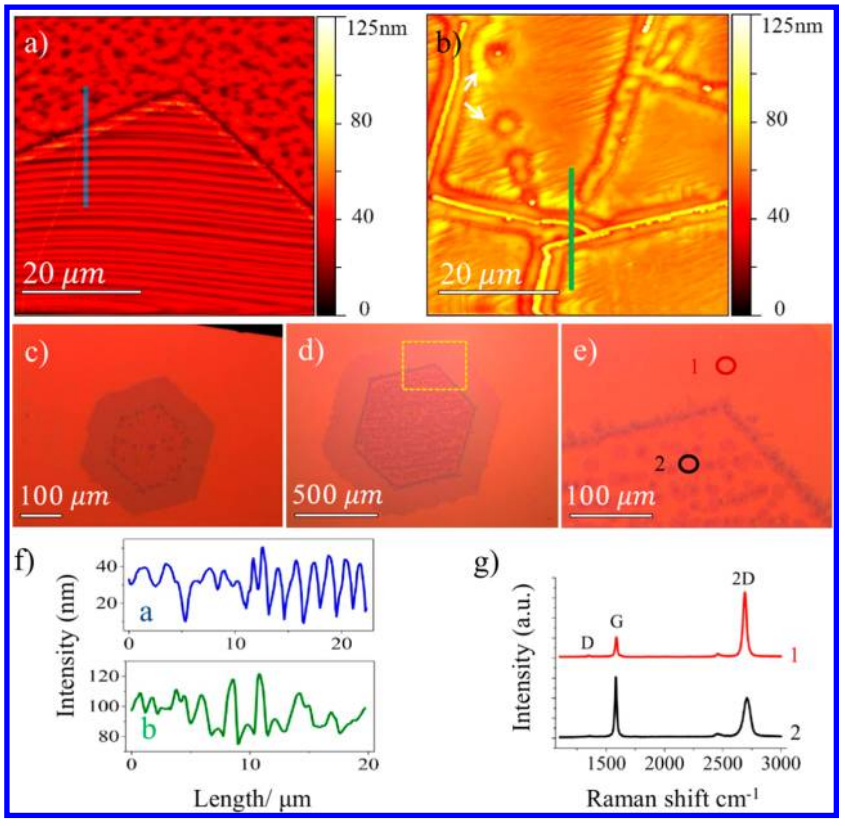

Figure 3. Surface morphology. AFM images for seed grain on (a) before and (b) after the fast heating treatment, respectively. Ring type etching holes (white arrows) are the typical characteristics of oxidation etching. (c, d) Optical images for grains regrown from slightly and heavily oxidized copper substrates, respectively. (e) Zoomed area in (d). (f) Height profiles for lines (a) and (b), respectively. (g) Raman spectra taken from sites 1 and 2 in (e).

graphene,[19] consistent with optical images in Figure 1c. Moreover, the intensity profile along the indicated line connecting the dots in first- and second-order diffraction pattern, as shown in the top panel of Figure 1f, reveals characteristics of monolayer graphene where the intensity at the first-order diffraction is about twice that of the second-order diffraction.[20,21] In contrast, SAED patterns obtained at the seed region (Figure 1h) show characteristic bilayer or few layers structures with AB stacking order,[20,21] consistent with optical observation in Figure 1c. When all the eight diffraction patterns are overlapped together (Figure 1i), they closely match with each other, suggesting single-lattice orientation in both of the seed and regrown regions. Slight lattice mismatch may arise from corrugation in grains or wrinkles introduced during the transfer process.[15,22,23] The AB stacking patterns, observed in the regrown region, are most likely originated from newly formed nuclei flakes in seed grain area during regrowth process, which will be discussed later. A small portion of non-AB stacking is sometimes also observed, which produces more than one set of SAED patterns, but normally, similar orientation coherence is observed (see data in Figure S6 in Supporting Information). Taken together, these SEAD results confirm the structure coherence in the seed grain and regrown region.

We further examined the evolution of graphene edges during regrowth process, as shown in Figure 2. Here a very short regrowth period was used to grow additional ∼6 μm in radius (a feature on the substrate was used as a reference point). Both graphene edges before and after the regrowth strictly follow the same line-shape, evidencing that the edges grow simultaneously at a similar rate, which confirms the observation that the regrowth is started from the edges of seed grain.

For continued growth of a large-area graphene grain from the edges of graphene seed, the following two requirements must be satisfied: (1) during the nucleation stage, nucleation energy barrier on the edges should be reduced, and thus the growth on those site are favored; (2) the overall nucleation density should be low so that the regrowth of grain would not be disrupted by newly forming of nucleus. It is reported experimentally that the activation energy of CH_4 decomposition is ∼125 kJ/mol when Cu (100) is covered with ∼0.5 monolayer oxygen, significantly lower than 201 kJ/mol on clean Cu (100) surface.[24] Therefore, if one can control the morphology of the oxide and guide them to distribute mostly at edges of graphene seeds, we should be able to confine the continued growth at those regions and simultaneously avoid formation of a large number of new nucleation sites, which otherwise would compete with the continued growth. Keeping in consideration, the key measure of our continued growth is a surface treatment method immediately applied before the second CVD growth, as explained in the Experimental Section. Additionally, morphology of the graphene/Cu surface after the surface treatment is monitored using atomic force microscopy (AFM). Figures 3a,b depict the AFM images before and after the surface treatment, respectively. Typically, the original CVD-grown graphene gains without oxidation shows a uniform film with periodical ripples, resulted from the thermal expansion coefficient mismatch between graphene and substrate.[1] However, after the surface treatment, a large quantity of new features, including cracks and ring-shape etching pits (see arrows in Figure 3b), appear on the

dx.doi.org/10.1021/cm501184s | Chem. Mater. 2014, 26, 4137−4143

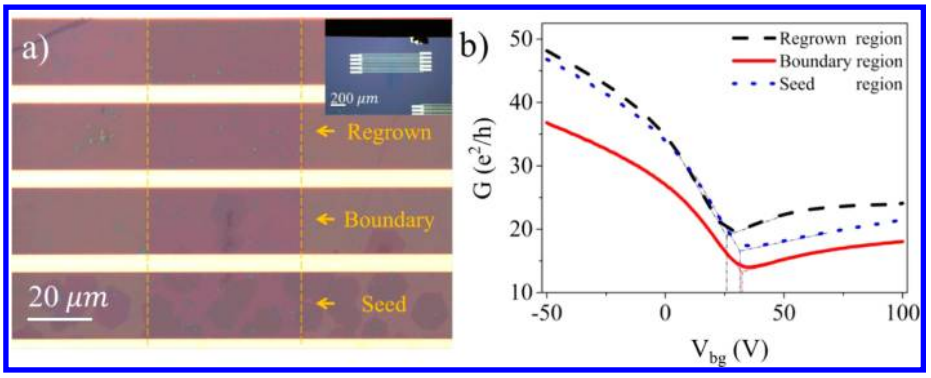

Figure 4. Electronic transport measurement. (a) Optical image of FET device along the boundary of seed and regrown grain. Dashed lines are used as guides for the edge of the graphene channels. Inset shows the images of all devices. (b) Conductance of graphene versus back gate voltage for graphene strips in seed, boundary, and regrown area.

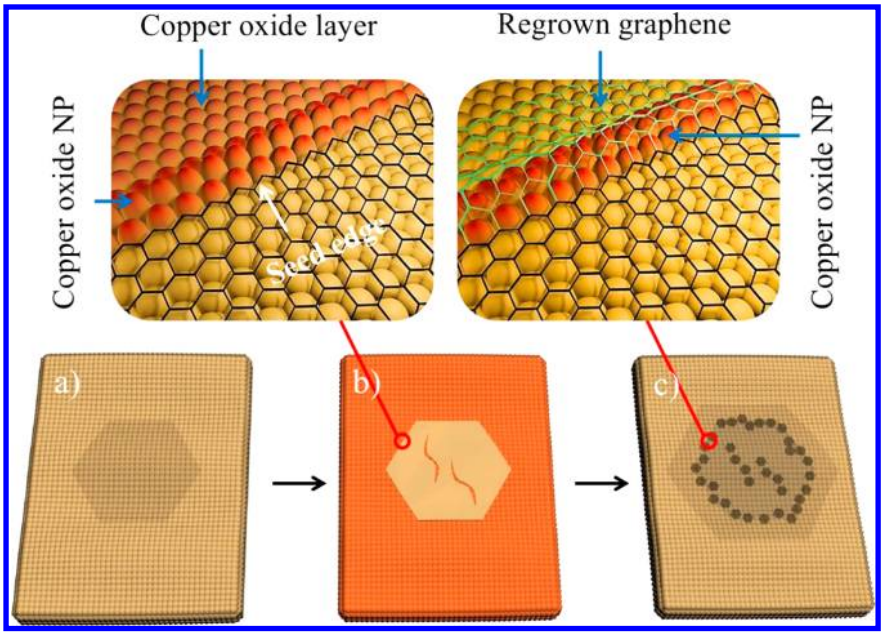

Figure 5. A schematic diagram (chemical structures and size are not to scale) of a continued growth process. (a) Single-crystalline grains are first synthesized on copper substrate. (b) Introduction of oxides nanoparticles into seed grain through oxidation of copper substrate by fast heating. Inset shows the formation of nanoparticles along the edge of seed grain. (c) Finally, continued growth is achieved by growth from the edges but which inevitably leads to new nucleus formation in other oxidized regions.

surface, resemble typical morphology of oxygen etching.[25,26] Such features are reported to be directly resulted from oxidation at reactive sites such as defects, boundaries, or wrinkles, which eventually disrupt graphene into fragments, pits, and cracks.[27,28] Indeed, the number of cracks and pits in seed is positively correlated with the degree of oxidation, that is, higher degree of oxidation induces higher density of cracks and pits (Figure S7). Consequently, copper surface initially protected by graphene becomes exposing and will likewise form oxides, similar to those observed in oxide-assisted seeded growth,[8] as previously reported.[29,30] A closer inspection at the graphene edges reveals that oxide nanoparticles tend to aggregate at the vicinities of edges, as shown in Figure 3b. The aggregation is also confirmed by the height profile shown in Figure 3f, where the nanoparticle height increases from ∼10 to ∼40 nm after oxidation. The XPS spectra, depicted in Figure S10 of Supporting Information, confirmed that the oxygen moieties resulted from this treatment are mostly confined in Cu_2O and CuO, consistent with previous study.[8,29] In addition, we did not observe significant morphology change, shown in Figure S10 in Supporting Information, when high-purity Cu foil was used, indicating those nanoparticles are not formed by oxidation of impurities in copper.

To elucidate the role of those oxides in the continued growth, we vary the duration of surface oxidation, and then investigate their effects on consequent second growth. Figure 3c,d demonstrates two regrown graphene grains synthesized with low and high degree of oxidation, respectively, and further transferred onto silicon wafers. As Figure 3c,d reveals, a drastic increase in nucleation density (i.e., high density of small flakes in the seed region) is seen when the starting surface is heavily oxidized (Figure 3d), as compared to slightly oxidization surface (Figure 3c). The observation of higher nucleation in high-degree-oxidized area (i.e., edges and cracks) is consistent with those observed in seeded growth,[8] where an oxidized nanoparticle of certain size is more likely to initiate the nucleation and also consistent with aforementioned reduction of activation energy on oxides. Raman spectra, shown in Figure 3g, show dominantly bilayer and monolayer, respectively, in the

dx.doi.org/10.1021/cm501184s | Chem. Mater. 2014, 26, 4137−4143

seed and regrown region, also consistent with the aforementioned optical images and SAED results.

We have demonstrated a CVD protocol for continued growth to enable the amplification of graphene grains. We further investigate whether the continued growth enable structure coherence and long-range electronic continuity. For this purpose, field effect transistors (FET) along boundary regions between the seed and regrown area are fabricated, shown in the inset of Figure 4. Before the fabrication of the FET devices, electron lithography followed by oxygen plasma etching is used to etch away the majorities of graphene film and leave only a stripe of film with ∼50 μm width, area shown between the dashed lines in Figure 4a. After that, a set of parallel electrodes is defined perpendicularly to the graphene stripe with equal distance of 20 μm between two electrodes, followed by deposition of Cr/Au (5 nm/70 nm) using E-beam evaporation and then lift-off in acetone. Electronic transport measurements on those devices are conducted in a cryostat under a vacuum pressure of around 10^{-6} Torr. Figure 4b plots the conductance (G, in unites of e^2/h) as a function of backgate voltage (V_{bg}) for graphene channels of the seed, the boundary and the regrowth region, respectively. All of these curves show a typical Dirac point for graphene materials,[31] corresponding to the minima in conductance, suggesting graphene produced in method are of high quality. More importantly, these results, along with the fact of electronic conductivity in the boundary region, provide strong evidence to support that structure coherence is kept even in the boundary regions. Slight shift among the positions of Dirac points may be due to the doping effect from oxygen trapped underneath the graphene or PMMA residue during transfer process. This is in agreement with AFM images and Raman mapping results, where no significant D peak intensity and cracks are observed in the boundary regions (see Figures S8 and S9 in Supporting Information).

On the basis of those above-mentioned observations, a tentative mechanism is presented to describe the continued growth processes for large-size graphene, as shown in Figure 5. First, single-crystalline graphene grain with ultralow density is synthesized by a previously reported method.[6−8] Second, fast heating in an Ar environment introduces oxide nanoparticles into copper surface, but that is mostly confined in the graphene seed edges. The assembling of oxide nanoparticles along edges might be attributed to the high activity of edges.[32−34] Inevitably, some parts of the seed grain on copper are also attacked by oxygen and become partially torn and broken, which lead to the formation of pits and cracks on the surface. Consequently, copper in those broken regions are also oxidized. In the final stage, those newly formed nanoparticles act as nucleation sites, as the energy barrier for methane decompostion become significantly reduced, resulting in the formation of new nuclei along the seed graphene edges and cracks, concurrently initiating the regrowth from those edges. In other words, the role of nanoparticles is to ensure the seed edges to be favored during growth and thus enables the structure amplification, similar to noncatalyst continued growth of carbon nanotube.[35]

In summary, we demonstrated a continued growth method to amplify the size of single-crystalline graphene in chemical vapor deposition. We observed that the oxides nanoparticles introduced by fast heating tend to aggregate on the graphene edges, as well as cracks and torn region. Utilizing the reduced energy barrier for methane decomposition in those sites, we were able to confine the nucleation and continued growth dominantly in those areas, which leads to the continued growth and eventually amplifies graphene sizes to millimeter size. TEM, Raman and electronic transport measurement specify that the regrown single-crystalline grain maintains lattice structure, shape, and orientation of the seed graphene. This continued growth concept could be applied to similar 2D materials synthesis, such as BN sheet and MoS_2, as well as their hybrid materials, to obtain large single-crystal materials with structure coherence.

■ ASSOCIATED CONTENT

Supporting Information

Additional information including a scheme for the growth process, optical/AFM images, Raman spectra, and XPS data. This material is available free of charge via the Internet at http://pubs.acs.org.

■ AUTHOR INFORMATION

Corresponding Author

*Email: keztluo@ust.hk.

Notes

The authors declare no competing financial interest.

■ ACKNOWLEDGMENTS

This project is supported by the Research Grant Council of Hong Kong SAR (project no. 623512 and DAG12EG05). Technical assistance from the Materials Characterization and Preparation Facilities is greatly appreciated. We thank VILLAROMAN Daniel and Baoling Huang at UST for assistance in electronic measurement.

■ REFERENCES

(1) Li, X. S.; Cai, W. W.; An, J. H.; Kim, S.; Nah, J.; Yang, D. X.; Piner, R.; Velamakanni, A.; Jung, I.; Tutuc, E.; Banerjee, S. K.; Colombo, L.; Ruoff, R. S. *Science* **2009**, *324*, 1312−1314.

(2) Kobayashi, T.; Bando, M.; Kimura, N.; Shimizu, K.; Kadono, K.; Umezu, N.; Miyahara, K.; Hayazaki, S.; Nagai, S.; Mizuguchi, Y.; Murakami, Y.; Hobara, D. *Appl. Phys. Lett.* **2013**, *102*, 023112.

(3) Han, G. H.; Gunes, F.; Bae, J. J.; Kim, E. S.; Chae, S. J.; Shin, H. J.; Choi, J. Y.; Pribat, D.; Lee, Y. H. *Nano Lett.* **2011**, *11*, 4144−4148.

(4) Gao, L.; Guest, J. R.; Guisinger, N. P. *Nano Lett.* **2010**, *10*, 3512−3516.

(5) Huang, P. Y.; Ruiz-Vargas, C. S.; van der Zande, A. M.; Whitney, W. S.; Levendorf, M. P.; Kevek, J. W.; Garg, S.; Alden, J. S.; Hustedt, C. J.; Zhu, Y.; Park, J.; McEuen, P. L.; Muller, D. A. *Nature* **2011**, *469*, 389−392.

(6) Hao, Y. F.; Bharathi, M. S.; Wang, L.; Liu, Y. Y.; Chen, H.; Nie, S.; Wang, X. H.; Chou, H.; Tan, C.; Fallahazad, B.; Ramanarayan, H.; Magnuson, C. W.; Tutuc, E.; Yakobson, B. I.; McCarty, K. F.; Zhang, Y. W.; Kim, P.; Hone, J.; Colombo, L.; Ruoff, R. S. *Science* **2013**, *342*, 720−723.

(7) Zhou, H. L.; Yu, W. J.; Liu, L. X.; Cheng, R.; Chen, Y.; Huang, X. Q.; Liu, Y.; Wang, Y.; Huang, Y.; Duan, X. F. *Nat. Commun.* **2013**, *4*, 2096.

(8) Lin, G.; Zhengtang, L. *ACS Nano* **2013**, *7*, 9480−9488.

(9) Ren, Z. F. *Nat. Nanotechnol.* **2007**, *2*, 17−18.

(10) Han, G. H.; Rodriguez-Manzo, J. A.; Lee, C. W.; Kybert, N. J.; Lerner, M. B.; Qi, Z. J.; Dattoli, E. N.; Rappe, A. M.; Drndic, M.; Johnson, A. T. C. *ACS Nano* **2013**, *7*, 10129−10138.

(11) Huang, J. F.; Larisika, M.; Fam, W. H. D.; He, Q. Y.; Nimmo, M. A.; Nowak, C.; Tok, I. Y. A. *Nanoscale* **2013**, *5*, 2945−2951.

(12) Liu, L.; Park, J.; Siegel, D. A.; McCarty, K. F.; Clark, K. W.; Deng, W.; Basile, L.; Idrobo, J. C.; Li, A. P.; Gu, G. *Science* **2014**, *343*, 163−167.

(13) Yan, K.; Wu, D.; Peng, H. L.; Jin, L.; Fu, Q.; Bao, X. H.; Liu, Z. F. *Nat. Commun.* **2012**, *3*, 1280.
(14) Li, X. S.; Magnuson, C. W.; Venugopal, A.; An, J. H.; Suk, J. W.; Han, B. Y.; Borysiak, M.; Cai, W. W.; Velamakanni, A.; Zhu, Y. W.; Fu, L. F.; Vogel, E. M.; Voelkl, E.; Colombo, L.; Ruoff, R. S. *Nano Lett.* **2010**, *10*, 4328−4334.
(15) Li, X. S.; Magnuson, C. W.; Venugopal, A.; Tromp, R. M.; Hannon, J. B.; Vogel, E. M.; Colombo, L.; Ruoff, R. S. *J. Am. Chem. Soc.* **2011**, *133*, 2816−2819.
(16) Jia, C. C.; Jiang, J. L.; Gan, L.; Guo, X. F. *Sci. Rep.* **2012**, *2*, 707.
(17) Vlassiouk, I.; Regmi, M.; Fulvio, P. F.; Dai, S.; Datskos, P.; Eres, G.; Smirnov, S. *ACS Nano* **2011**, *5*, 6069−6076.
(18) Wood, J. D.; Schmucker, S. W.; Lyons, A. S.; Pop, E.; Lyding, J. W. *Nano Lett.* **2011**, *11*, 4547−4554.
(19) Yan, Z.; Lin, J.; Peng, Z. W.; Sun, Z. Z.; Zhu, Y.; Li, L.; Xiang, C. S.; Samuel, E. L.; Kittrell, C.; Tour, J. M. *ACS Nano* **2012**, *6*, 9110−9117.
(20) Ferrari, A. C.; Meyer, J. C.; Scardaci, V.; Casiraghi, C.; Lazzeri, M.; Mauri, F.; Piscanec, S.; Jiang, D.; Novoselov, K. S.; Roth, S.; Geim, A. K. *Phys. Rev. Lett.* **2006**, *97*, 187401.
(21) Meyer, J. C.; Geim, A. K.; Katsnelson, M. I.; Novoselov, K. S.; Booth, T. J.; Roth, S. *Nature* **2007**, *446*, 60−63.
(22) Yu, Q. K.; Jauregui, L. A.; Wu, W.; Colby, R.; Tian, J. F.; Su, Z. H.; Cao, H. L.; Liu, Z. H.; Pandey, D.; Wei, D. G.; Chung, T. F.; Peng, P.; Guisinger, N. P.; Stach, E. A.; Bao, J. M.; Pei, S. S.; Chen, Y. P. *Nat. Mater.* **2011**, *10*, 443−449.
(23) Wang, H.; Wang, G. Z.; Bao, P. F.; Yang, S. L.; Zhu, W.; Xie, X.; Zhang, W. J. *J. Am. Chem. Soc.* **2012**, *134*, 3627−3630.
(24) Alstrup, I.; Chorkendorff, I.; Ullmann, S. *Surf. Sci.* **1992**, *264*, 95−102.
(25) Liu, L.; Ryu, S. M.; Tomasik, M. R.; Stolyarova, E.; Jung, N.; Hybertsen, M. S.; Steigerwald, M. L.; Brus, L. E.; Flynn, G. W. *Nano Lett.* **2008**, *8*, 1965−1970.
(26) Lemaitre, M. G.; Donoghue, E. P.; McCarthy, M. A.; Liu, B.; Tongay, S.; Gila, B.; Kumar, P.; Singh, R. K.; Appleton, B. R.; Rinzler, A. G. *ACS Nano* **2012**, *6*, 9095−9102.
(27) Duong, D. L.; Han, G. H.; Lee, S. M.; Gunes, F.; Kim, E. S.; Kim, S. T.; Kim, H.; Ta, Q. H.; So, K. P.; Yoon, S. J.; Chae, S. J.; Jo, Y. W.; Park, M. H.; Chae, S. H.; Lim, S. C.; Choi, J. Y.; Lee, Y. H. *Nature* **2012**, *490*, 235−239.
(28) Starodub, E.; Bartelt, N. C.; McCarty, K. F. *J. Phys. Chem. C* **2010**, *114*, 5134−5140.
(29) Jiang, X. C.; Herricks, T.; Xia, Y. N. *Nano Lett.* **2002**, *2*, 1333−1338.
(30) Hsieh, Y. P.; Hofmann, M.; Chang, K. W.; Jhu, J. G.; Li, Y. Y.; Chen, K. Y.; Yang, C. C.; Chang, W. S.; Chen, L. C. *ACS Nano* **2014**, *8*, 443−448.
(31) Novoselov, K. S.; Geim, A. K.; Morozov, S. V.; Jiang, D.; Zhang, Y.; Dubonos, S. V.; Grigorieva, I. V.; Firsov, A. A. *Science* **2004**, *306*, 666−669.
(32) Wang, X. R.; Li, X. L.; Zhang, L.; Yoon, Y.; Weber, P. K.; Wang, H. L.; Guo, J.; Dai, H. J. *Science* **2009**, *324*, 768−771.
(33) Koskinen, P.; Malola, S.; Hakkinen, H. *Phys. Rev. Lett.* **2008**, *101*, 115502.
(34) Koskinen, P.; Malola, S.; Hakkinen, H. *Phys. Rev. B* **2009**, *80*, 073401.
(35) Yao, Y. G.; Feng, C. Q.; Zhang, J.; Liu, Z. F. *Nano Lett.* **2009**, *9*, 1673−1677.